Int J Earth Sci (Geol Rundsch)
DOI 10.1007/s00531-006-0136-0

ORIGINAL PAPER

Latest Precambrian to Early Cambrian U–Pb zircon ages of augen gneisses from Calabria (Italy), with inference to the Alboran microplate in the evolution of the peri-Gondwana terranes

Francesca Micheletti · Pierre Barbey · Annamaria Fornelli · Giuseppe Piccarreta · Etienne Deloule

Received: 30 May 2006 / Accepted: 20 October 2006
© Springer-Verlag 2006

Abstract In situ U–Pb dating of zircons from five samples of Calabrian augen gneisses shows that their protoliths are Latest Precambrian to Early Cambrian in age (562 ± 15, 547 ± 7, 540 ± 4, 539 ± 16 and 526 ± 10 Ma), and contain Archaean (3.1 Ga), Palaeoproterozoic (1.7–2.4 Ga) and Neoproterozoic (0.6–0.9 Ga) inheritance. Geochemical signature of augen gneisses is typical of high-K calc-alkaline post-collisional magmatism. Their Sr–Nd isotopic compositions [$0.7093 < (^{87}Sr/^{86}Sr)_i < 0.7139$; $-3.2 < \varepsilon_{Nd(t)} < -5.4$; $1.5 < T_{DM} < 1.7$ Ga] indicate the involvement of a crustal component in significant proportions. The Calabrian augen gneisses have, therefore, to be distinguished from the orthogneisses of Sardinia and northern Algeria, and from the porphyroids of Sicily, which are Middle Ordovician. By contrast, the Calabrian augen gneisses show a close similarity to the Pan-African post-collisional granitoids of the northern edge of the West African craton (e.g. the Moroccan Anti-Atlas). This suggests a peri-Gondwana origin and corroborates previous palaeogeodynamic reconstructions attributing the Alboran microplate to the northern margin of the West African craton.

F. Micheletti (✉) · A. Fornelli · G. Piccarreta
Dipartimento Geomineralogico, Bari University,
via Orabona 4, 70125 Bari, Italy
e-mail: f.micheletti@geomin.uniba.it

P. Barbey · E. Deloule
CRPG-CNRS, B. P. 20,
54501 Vandoeuvre-lès-Nancy Cedex, France

Keywords Latest Precambrian to Early Cambrian · Calabria · Alboran microplate · U–Pb dating · Zircon

Introduction

Large bodies of granitic orthogneisses occur in most segments of the European Variscan belt, from the Central Iberian Zone in Spain to the Bohemian Massif. Two groups of orthogneisses can be distinguished on the base of zircon U–Pb emplacement ages (Table 1): (1) mainly Latest Precambrian–Early Cambrian in central and eastern Europe, and (2) mainly upper Cambrian to middle Ordovician in western Europe. The Alboran microplate (Andrieux et al. 1971), or AlKaPeca (Bouillin et al. 1986), which is inferred to have occupied a central position within the peri-Gondwana Cadomian terranes (e.g. Stampfli and Borel 2002; von Raumer et al. 2002), is now considered to be fragmented within the Alpine and Variscan chains of southern Europe and North Africa (Calabria, Peloritani Mountains, Sardinia, southern Spain, Maghrebides). These fragments also contain large masses of orthogneisses, which occur in Sardinia, Calabria (Italy) and northern Algeria. A few available age data show that these orthogneisses range from lower Ordovician in Sardinia (Giacomini et al. 2006) and Petite Kabylie (Peucat et al. 1996), to Neoproterozoic-Early Cambrian in Calabria (Aspromonte and Serre; Schenk and Todt 1989; Senesi 1999). Middle Ordovician silicic and mafic metavolcanic rocks are also present in southern Calabria and in the Peloritani Mountains (paleontological records: Acquafredda et al. 1994; U–Pb zircon ages: Trombetta et al. 2004). However, large bodies of

Table 1 U–Pb zircon ages of orthogneisses from the European Variscan belt (see also von Raumer et al. 2002; Dörr et al. 2004)

Location	Ages (Ma)	References
Latest Precambrian–Early Cambrian		
Iberian Peninsula (Spain and Portugal)		
Calc-alkaline orthogneisses	590–510	Ochsner (1993)
Massif Central (France)		
Aubrac metadiorites	540 (id)	Pin and Lancelot (1978)
Maures Massif (France)		
Leptynites	548 + 15/–7 (id)	Innocent et al. (2003)
Bohemian Massif (Czech Republic)		
Tepla crystalline complex	513 + 7 (id)	Dörr et al. (1998)
Erzebirge (Saxony and Czech Republic)		
Inner grey gneisses	541 ± 4 (id), 528 ± 6 (pd) 550 ± 7, 555 ± 7 (Pb)	Tichomirowa et al. (2001) Kröner et al. (1995)
Red gneisses	480–500 (Pb) 550 ± 9, 554 ± 10 (Pb)	Tichomirowa et al. (2001) Kröner et al. (1995)
Eastern Alps (Austria)		
Silvretta Nappe older orthogneiss	519 ± 7, 526 ± 7, 533 ± 4, 568 ± 6, 532 ± 30 (id, Pb)	Muller et al. (1995), (1996)
Felbertal	529 + 18 (pd)	Eichhorn et al. (1999)
South Carpathians (Romania)		
Lainici –Paius Group	567–588 (id)	Liégeois et al. (1996)
Calabria (Italy)		
Serre	549 ± 4 (id)	Senesi (1999)
Aspromonte	516 ± 25, 622 ± 120 (id)	Schenk and Todt (1989)
Upper Cambrian- Middle Ordovician		
Galicia (Spain)		
Malpica-Tuy	480 ± 2 (id)	Santos Zalduegui et al. (1995)
Ordones Complex	500 ± 2 (id)	Abati et al. (1999)
Central Iberian Zone (Spain)		
Ollo de Sapo	468–488 (id)	Valverde-Vaquero and Dunning (2000)
Eastern Pyrenees/Montagne Noire (France)		
Canigou, Nuria, Roc de France	461 ± 7–477 ± 4 (pd)	References in Laumonier et al. (2004)
Axial zone	456 + 3, 471 + 4 (id)	Roger et al. (2004); Cocherie et al. (2005)
Armorican massif (France)		
Cellier unit	481 ± 6 (id)	Ballévre et al. (2002)
Saint-Mars du Désert, Moëlan, Tréauray	485 ± 11 (id), 485 ± 6, 466 ± 12 (id)	References in Jegouzo et al. (1986)
Western Alps (Switzerland)		
Thyon metagranite	500 ± 4 (id)	Bussy et al. (1996)
Various porphyritic metagranites	438–462 (id)	References in Bussy et al. (1996)
Ruitor gneisses	460 ± 7, 465 ± 11(id)	Guillot et al. (2002)
Eastern Alps (Austria)		
Boulders in Kalwang Conglomerate	ca. 502 ± 17 (id)	Neubauer et al. (2002)
Black Forest (Germany)		
Moldanubian gneisses	497 ± 3–506 ± 6 (Pb)	Chen et al. (2000)
West Sudetes (Poland, Czech Republic)		
Orlica-Snieznik gneisses	495 ± 14 (pd)	Turniak et al. (2000)
Bohemian Massif (Czech Republic)		
Domazlice complex	480 ± 9 (id)	Glodny et al. (1998)
Sardinia		
North Sardinia orthogneisses	469 ± 4, 464 ± 1 (pd)	Giacomini et al. (2006)

id U–Pb isotopic dilution, *pd* U–Pb punctual dating on zircon, *Pb* Pb–Pb evaporation technique

orthogneisses, belonging to different tectonic units of the Tertiary nappe-structured edifice of Calabria–Peloritani including pre-Triassic rocks, remains of unknown age. Moreover, there is no clear evidence, up to now, of Precambrian basement in Calabria and the oldest metasediments reported in Calabria are Cambrian to Devonian in age (Stilo and Bocchigliero units; Acquafredda et al. 1994).

This paper presents new geochemical and geochronological data on augen gneisses from the Castagna, Sila and Aspromonte tectonic units, in Calabria. Our aim is (1) to constrain emplacement ages and geochemical features of the augen gneisses; (2) obtain information about inheritance from older sources; and (3) to discuss their significance with respect to the organization of the pre-Variscan basement areas

(especially the Alboran microplate) at the north-Gondwana margin (von Raumer et al. 2002).

Geological setting

Calabria together with the Peloritani Mountains represents a segment of the Alpine chain connecting the NW–SE-trending Apennines to the E–W-trending Sicilian Maghrebides (Fig. 1). The Calabria–Peloritani orogenic belt is considered as an ''exotic terrane'' consisting of tectonic units stacked during the Alpine orogeny (Bonardi et al. 2001; Festa et al. 2004). They include from the top: (1) pre-Triassic basement rocks with remnants of sedimentary cover; (2) fragments of Jurassic to lower Cretaceous Tethyan oceanic crust; and (3) Mesozoic to Cenozoic sedimentary rocks (e.g. Amodio Morelli et al. 1976; Bouillin 1984). South of the Cenozoic Catanzaro Graben, only units of Variscan continental crust covered by Mesozoic to Cenozoic sedimentary rocks are exposed. The basement rocks (Fig. 1) outcrop mainly in Catena Costiera, Sila and Serre Massifs, Capo Vaticano Promontory, Aspromonte Massif (Calabria) and in the Peloritani Mountains (Sicily). The provenance of the rootless crystalline nappes is still debated. They have been interpreted as fragment of either the African margin (e.g. Amodio-Morelli et al. 1976; Grandjacquet and Mascle 1978), or the European continental margin (Boullin et al. 1986; Dietrich 1988), or a microplate located between the European and the African continental margins (Guerrera et al. 1993; Bonardi et al. 1996). The present tectonic setting of the Calabria–Peloritani segment is the result of pre-Variscan to Cenozoic events (Schenk 1990; Thomson 1994; Caggianelli et al. 2000; Del Moro et al. 2000; Festa et al. 2003). Two distinct models have been proposed for its tectonic evolution:

1. Building of a Cretaceous-Paleogene Europe-verging chain, which was thrust onto Africa-verging Apennine units during early Miocene (e.g. Amodio Morelli et al. 1976).
2. Stacking of European and Tethyan units, which were subsequently thrust onto the Africa continental margin in the early Miocene (e.g. Boullin 1984).

The pre-Triassic basement rocks include large masses of silicic augen gneisses associated with metasediments belonging to the upper, middle and lower segments of the Variscan continental crust: the Castagna, Aspromonte and Sila Units, respectively. The Castagna and Sila Units crop out in the Catena Costiera, Sila and northern Serre, whereas the Aspromonte Unit crops out in the Aspromonte Massif and in the Peloritani Mountains (Fig. 1). Field relationships show that the augen gneisses were once intrusive in older metasedimentary series. The augen gneisses consist dominantly of quartz, K-feldspar (both in the matrix and as megacrysts), plagioclase, biotite and, locally, muscovite or garnet and sillimanite. Common accessory phases are epidote, tourmaline, zircon and apatite. Phase assemblages in both augen gneisses and associated metasediments indicate equilibration under low- to high-grade conditions during the Variscan metamorphism (e.g. Bonardi et al. 1984; Schenk 1990;

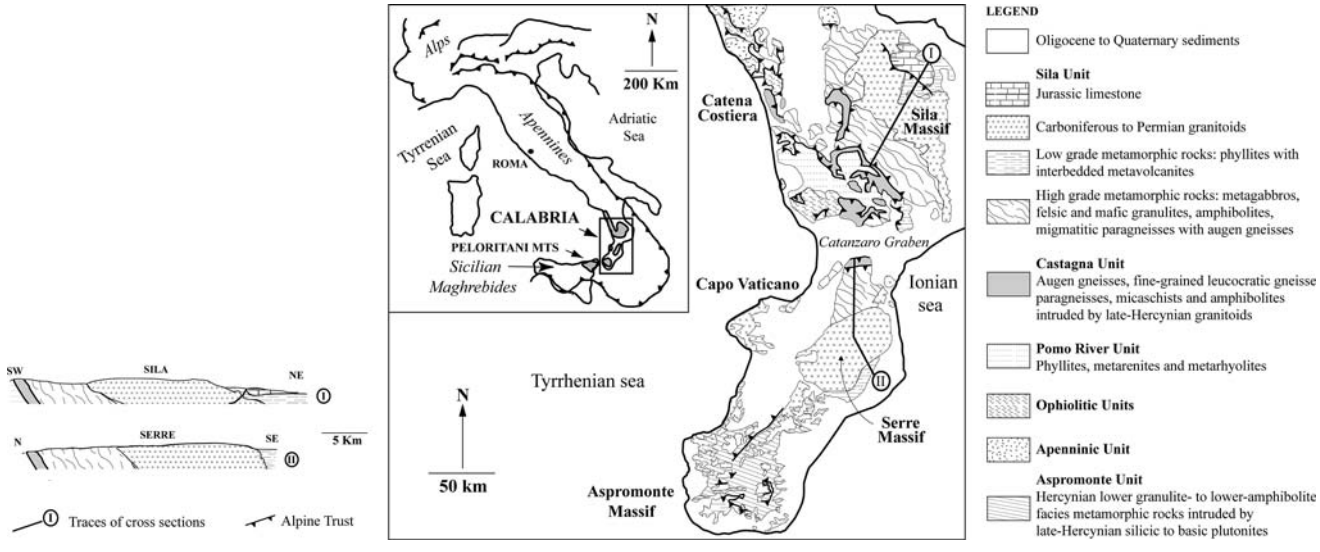


Fig. 1 Geological sketch map of Calabria (modified from Festa et al. 2004)

Fornelli et al. 2002): greenschist to amphibolite facies in the Castagna Unit, amphibolite facies in the Aspromonte Unit, and amphibolite to granulite facies in the Sila Unit. The augen gneisses were locally reworked during the Alpine tectonic events, with development of mylonites (Colonna and Piccarreta 1975; Paglionico and Piccarreta 1976; Piccarreta 1981; Bonardi et al. 1984, 1996; Platt and Compagnoni 1990; Prosser et al. 2003).

The schematic organization of the nappe structured Alpine edifice south of the Catanzaro Graben, is shown in Fig. 2. The Castagna Unit is tectonically superimposed on the phyllitic Pomo River Unit and underlies the Sila Unit. The Aspromonte Unit is tectonically sandwiched between greenschist-facies lower units and the upper Stilo Unit comprising greenschist to amphibolite-facies metamorphic rocks intruded by late-Variscan granitoids (Bonardi et al. 1984). In the Castagna Unit, the voluminous augen gneisses are associated with minute leucocratic orthogneisses, garnet-biotite-muscovite paragneisses, micaschists (locally sillimanite-bearing), amphibole-bearing paragneisses and minor quartzites, amphibolites, calc-silicate rocks and marbles (Colonna and Piccarreta 1975; Paglionico and Piccarreta 1976). In the Sila Unit (Serre Massif), the augen gneisses form decametre- to hectometre-sized lenses within migmatitic metapelites containing intercalations of mafic granulites. In the Aspromonte Unit, huge masses of augen gneisses are associated with biotite–sillimanite–garnet paragneisses and micaschists, minute leucocratic gneisses, amphibole-bearing gneisses, amphibolites, meta-ultramafic rocks, calc-silicate rocks and marbles (Bonardi et al. 1984 and references therein).

The augen gneisses within the three units are crosscut by late-Variscan granitoids and pegmatites. Three multigrain U–Pb zircon analyses from the augen gneisses of the Sila and Aspromonte Units are available and yield Pan-African emplacement ages (549 ± 4 Ma in Senesi 1999; 516 ± 25 and 622 ± 120 Ma in Schenk and Todt 1989).

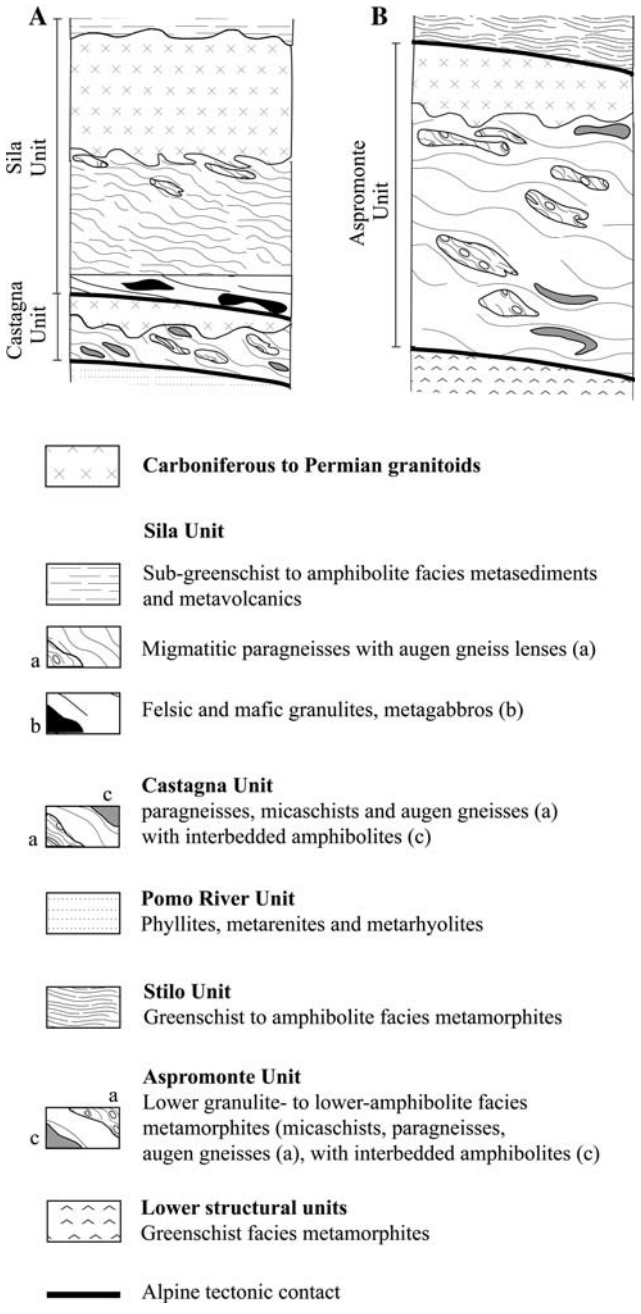


Fig. 2 Synthetic structural sections in Sila and northern Serre (**a**), and in Aspromonte (**b**). Modified from Festa et al. (2004)

Major-trace elements and Sr–Nd isotopic compositions

Thirty-nine samples collected in the three units were analysed for major and trace elements (Tables 2 and 3). Major and some trace elements (Ba, Rb, Sr, Y, Zr, Nb, Ni, Cr, V) were determined by XRF spectrometry from powdered rock samples (Dipartimento Geomineralogico, Bari University). The other trace elements were measured by inductively coupled plasma mass spectrometry (ICP-MS) at CRPG (Nancy, France), using HNO_3 solutions prepared from fused glass. Sample preparation, analytical conditions and limits of detection are found in Acquafredda et al. (1985) and Carignan et al. (2001), respectively. Nd–Sr isotopic compositions of six samples (Table 4) were determined on a Finnigan mass spectrometer MAT 262 at CRPG. Analytical procedures are given in Ayalew et al. (2002).

On the whole, the major elements of augen gneisses from the three structural units indicate a granitic

Table 2 Major (wt%) and trace (ppm) elements of augen gneisses from Calabria

	Castagna Unit																	Sila Unit		
	GO1	GO2	GO3	GO4	GO5	GO6	GO8	GO9	GO10	GO35	GO22	GO28	GO58	GO63	GO63a	GO6 3b	GO63c	GO71	GO73	GO99
SiO_2	69.89	70.33	68.91	69.29	69.99	69.51	68.31	69.27	70. 12	68.85	68.74	69.48	69.17	69.38	69.78	69.85	66.88	68.82	72.42	70.18
TiO_2	0.56	0.52	0.61	0.52	0.52	0.63	0.61	0.61	0.57	0. 73	0.68	0.58	0.49	0.46	0.50	0.43	0.74	0.66	0.45	0.64
Al_2O_3	14.59	14.68	15.10	15.25	14.97	14. 13	14.10	14.36	14.32	13.94	15.13	14.76	15.10	14.65	14.36	14.52	15.18	14. 58	13.50	13.88
FeO_T	3.02	2.07	3.06	3.08	3.20	3.39	3.34	3.52	3.39	3.85	3.20	3.45	2.72	2. 87	2.91	2.70	4.04	3.44	2.38	3.36
MnO	0.05	0.04	0.04	0.06	0.03	0.05	0.04	0.05	0.05	0.05	0.04	0.05	0.03	0. 04	0.04	0.03	0.05	0.05	0.03	0.06
MgO	1.67	1.53	1.55	1.12	1.23	1.58	1.72	1.72	1.51	1.97	1.60	1.44	1.22	1. 44	1.40	1.31	2.07	1.64	0.88	1.28
CaO	1.30	0.95	1.30	1.22	1.15	1.63	0.88	1.42	1.38	1.86	0.96	0.75	1.17	1. 30	1.42	1.35	1.78	1.91	0.89	1.88
Na_2O	2.91	2.39	2.97	3.69	3.24	3.10	2.92	3.47	3. 79	2.91	2.58	3.63	3.18	3.14	3.27	3.07	3.09	2.54	2.26	2.68
K_2O	3.89	5.91	4.70	3.48	3.06	4.46	3.97	3.59	3. 23	4.40	5.37	3.20	5.08	4.97	4.76	5.21	4.03	5.20	6.41	4.91
P_2O_5	0.09	0.08	0.12	0.11	0.07	0.10	0.09	0. 10	0.12	0.10	0.10	0.09	0.08	0.09	0.09	0.10	0.11	0.14	0.05	0.12
LOI	1.69	1.27	1.30	1.85	2.18	1.06	3.65	1.50	1.14	0.92	1.24	2.19	1.46	1. 34	1.16	1.13	1.59	0.64	0.47	0.64
Total	99.66	99.77	99.66	99.67	99.64	99.64	99.63	99.61	99.62	99.58	99.64	99.62	99.70	99.68	99.69	99.70	99.56	99.62	99.74	99.63
Ba	580	600	554	486	472	665	570	592	453	610	588	514	509	531	577	527	689	7 80	646	673
Rb	130	182	210	262	155	175	181	168	179	190	223	161	164	195	185	171	144	1 36	188	106
Sr	114	90	127	92	153	178	107	138	114	152	87	96	133	126	146	120	210	147	1 22	128
V	45	45	52	46	44	54	52	56	48	68	59	54	41	43	47	38	66	56	30	52
Cr	60	66	61	52	55	60	62	58	56	84	70	94	62	64	44	38	72	45	25	33
Ni	17	14	17	16	16	18	17	19	17	22	18	18	14	17	15	14	21	18	9	14
Nb	13	10	15	15	17	13	13	14	18	15	14	14	13	14	13	12	15	13	12	12
Hf	–	6.5	–	–	–	7.0	6.4	6.2	5.7	4.3	–	–	–	5.7	–	5.2	8.7	6.2	–	–
Ta	–	0.8	–	–	–	1.0	1.0	1.2	1.7	0.6	–	–	–	1.3	–	1.3	0.9	0.9	–	–
Pb	–	22	–	–	–	29	25	20	27	15	–	–	–	42	–	19	16	28	–	–
Th	–	20.2	–	–	–	20.6	20.1	19.7	19.6	12.3	–	–	–	17.9	–	16.4	25.3	19.3	–	–
U	–	4.4	–	–	–	3.9	6.5	3.7	4.8	1.6	–	–	–	2.6	–	2.1	1.4	2.4	–	–
Zr	205	214	216	205	218	231	223	240	215	259	215	225	177	191	210	165	279	2 23	144	220
Y	39	34	32	33	34	37	39	39	35	39	30	41	39	33	36	34	45	33	20	33
La	24.9	30.5	25.5	31.1	23.9	40.5	40.3	37.3	38.3	25.4	26.9	34.0	28.3	32. 6	23.0	31.0	50.1	41.8	25.4	27.2
Ce	50.3	65.1	45.7	58.5	49.8	80.0	75.3	74.9	76.5	50.3	49	63.3	59.2	66.3	43. 1	63.8	101.0	82.5	43.8	49.2
A/CNK	1.28	1.22	1.22	1.26	1.39	1.10	1.32	1.18	1.17	1.08	1.28	1.37	1.17	1. 13	1.09	1.10	1.20	1.10	1.10	1.06

	Sila Unit					Aspromonte Unit													
	GO100	GO106	GO107	GO110	GO111	GO112	GO117	GO118	GO121	GO122	ADR3	ADR4	ADR5	ADR10	ADR12	ADR13	ADR 18	ADR23a	ADR23b
SiO_2	69.31	68.71	70.62	72.71	70.18	70.14	72.10	71.80	71.76	70.85	72.55	67.46	71.29	72.89	74.50	72.16	70.88	70.00	71.70
TiO_2	0.69	0.73	0.54	0.43	0.60	0.74	0.42	0.46	0.46	0. 53	0.49	0.67	0.49	0.37	0.33	0.45	0.50	0.52	0.40
Al_2O_3	14.17	14.32	14.17	13.59	14.44	13. 38	13.51	13.92	13.22	13.32	14.19	16.88	13.24	13.18	12.46	13.83	13.80	14. 31	13.82
FeO_T	3.44	3.53	2.84	2.02	3.15	4.21	2.39	2.41	2.38	3.02	3.80	2.86	2.80	2. 42	2.23	2.34	2.97	2.94	2.71
MnO	0.05	0.06	0.04	0.01	0.04	0.05	0.05	0.05	0.04	0.05	0.08	0.09	0.05	0. 04	0.04	0.07	0.03	0.04	0.02
MgO	1.52	1.80	1.03	1.01	1.24	1.71	0.75	0.85	1.26	1.39	0.88	1.27	1.31	0. 82	0.56	1.69	2.06	1.23	1.07
CaO	1.85	1.73	1.76	0.88	2.28	1.82	0.83	0.85	0.89	0.94	0.97	1.43	1.59	0. 42	1.11	1.48	0.57	1.53	0.52
Na_2O	2.54	2.31	2.89	2.03	3.02	3.05	1.61	1.64	1. 22	2.26	0.80	1.32	1.65	1.21	3.04	1.78	1.61	2.96	2.85
K_2O	5.51	5.73	5.21	6.24	4.22	3.39	6.64	6.71	7. 29	6.18	3.97	5.81	6.56	6.94	4.51	4.06	5.66	4.85	5.22
P_2O_5	0.13	0.10	0.11	0.04	0.14	0.10	0.11	0. 11	0.10	0.11	0.12	0.11	0.12	0.12	0.08	0.11	0.11	0.09	0.10

Table 2 continued

	Sila Unit					Aspromonte Unit													
	GO100	GO106	GO107	GO110	GO111	GO112	GO117	GO118	GO121	GO122	ADR3	ADR4	ADR5	ADR10	ADR12	ADR13	ADR 18	ADR23a	ADR23b
LOI	0.41	0.60	0.47	0.82	0.34	0.96	1.32	0.94	1.11	1.03	1.72	1.78	0.59	1. 33	0.88	1.77	1.48	1.21	1.28
Total	99.62	99.62	99.68	99.78	99.65	99.55	99.73	99.74	99.73	99.68	99. 57	99.68	99.69	99.74	99.74	99.74	99.67	99.68	99.69
Ba	745	803	709	519	704	789	582	576	815	732	194	491	759	595	319	228	584	5 82	595
Rb	125	132	131	150	117	120	241	229	204	203	164	204	237	246	178	168	187	1 44	145
Sr	139	141	132	94	138	183	81	77	168	109	39	94	119	56	72	58	55	130	70
V	52	56	42	34	45	68	35	37	37	44	40	64	40	27	19	28	43	39	34
Cr	38	43	32	32	33	59	38	36	37	33	39	60	47	25	17	16	33	45	22
Ni	14	16	12	13	13	25	13	10	15	16	10	15	14	9	5	8	13	11	9
Nb	13	14	12	9	11	15	11	11	12	11	12	15	11	10	14	21	11	14	10
Hf	6.0	–	–	–	–	–	–	5.6	–	–	–	6.4	6.0	–	–	–	5.6	5.8	–
Ta	0.7	–	–	–	–	–	–	1.1	–	–	–	1.2	1.0	–	–	–	1.2	1.2	–
Pb	23	–	–	–	–	–	–	21	–	–	–	17	11	–	–	–	12	21	–
Th	21	–	–	–	–	–	–	20	–	–	–	23	19	–	–	–	19	21	–
U	1.6	–	–	–	–	–	–	4.4	–	–		4.4	3.9	–	–	–	3.9	5.3	–
Zr	188	201	172	150	159	289	206	181	184	179	190	248	184	151	149	224	179	1 91	151
Y	31	26	29	8	21	30	38	31	33	27	36	44	34	36	45	34	22	34	19
La	43.3	28.8	26.7	20.0	24.6	43.1	29.8	37.4	27.8	31.4	28.3	39.7	36.7	30. 6	48.9	39.9	31.1	36.9	32.9
Ce	84.5	42.8	47.6	31.9	46.5	81.1	53.9	76.3	49.2	56.9	52.2	80.0	74.4	44. 8	73.1	72.7	62.5	72.4	60.5
A/CNK	1.05	1.09	1.04	1.16	1.06	1.12	1.19	1.21	1.15	1.10	1.92	1.53	1.04	1. 28	1.05	1.38	1.41	1.11	1.22

FeO_T = total iron as Fe^{2+}, LOI = loss on ignition, A/CNK = $Al_2O_3/(CaO + Na_2O + K_2O)_{molar}$

Table 3 Rare earth elements (ppm) of augen gneisses from Calabria

	Castagna Unit									Sila Unit		Aspromonte Unit				
	GO2	GO6	GO8	GO9	GO10	GO35	GO63	GO63b	GO63c	GO71	GO100	GO118	ADR4	ADR5	ADR18	ADR23a
La	30.5	40.5	40.3	37.3	38.3	25.4	32.6	31.0	50.1	41.8	43.3	37.4	39.7	36.7	31.1	36.9
Ce	65.1	80.0	75.3	74.9	76.5	50.3	66.3	63.8	101.0	82.5	84.5	76.3	80.0	74.4	62.5	72.4
Pr	7.8	9.4	9.8	8.8	8.9	6.0	7.7	7.4	11.7	9.6	9.6	8.8	9.4	8.7	7.3	8.3
Nd	29.6	35.0	36.6	32.6	33.2	22.1	28.8	27.2	43.0	35.5	35.3	32.2	34.5	31.9	26.90	30.00
Sm	6.3	6.9	7.3	6.5	6.7	4.6	6.0	5.7	8.7	7.1	7.1	6.8	7.1	6.7	5.48	6.01
Eu	1.00	1.23	1.14	1.10	0.92	0.63	0.99	0.96	1.44	1.24	1.16	1.04	1.06	1.03	0.76	1.04
Gd	5.70	6.15	6.68	5.87	5.87	3.99	5.22	5.38	7.61	6.27	6.26	6.20	6.53	5.91	4.80	5.20
Tb	0.95	0.97	1.07	0.98	0.97	0.63	0.88	0.86	1.20	1.00	1.00	1.05	1.10	0.98	0.77	0.89
Dy	5.58	5.83	6.45	5.91	6.00	3.77	5.33	5.49	7.40	5.78	5.76	6.40	6.17	5.84	4.58	5.23
Ho	1.13	1.13	1.25	1.14	1.13	0.74	1.00	1.03	1.43	1.15	1.13	1.24	1.24	1.16	0.89	1.07
Er	3.20	3.17	3.45	3.27	3.25	2.11	2.84	2.94	3.89	3.23	3.18	3.45	3.41	3.36	2.50	3.00
Tm	0.49	0.49	0.50	0.49	0.49	0.30	0.42	0.44	0.54	0.48	0.47	0.51	0.52	0.49	0.38	0.49
Yb	3.31	2.88	3.24	3.09	3.06	1.93	2.72	2.82	3.17	3.22	3.15	3.11	3.53	3.28	2.53	3.47
Lu	0.49	0.43	0.47	0.43	0.43	0.29	0.39	0.42	0.50	0.49	0.47	0.45	0.52	0.48	0.38	0.53
Eu/Eu*	0.51	0.58	0.50	0.55	0.45	0.45	0.54	0.53	0.54	0.57	0.53	0.49	0.48	0.50	0.45	0.57

Table 4 Sr–Nd isotopic compositions of augen gneisses from Calabria

Sample	Rb (ppm)	Sr (ppm)	$^{87}Rb/^{86}Sr$ (ppm)	$^{87}Sr/^{86}Sr$ (ppm)	$(^{87}Sr/^{86}Sr)_i$ (ppm)	Nd (ppm)	Sm (ppm)	$^{147}Sm/^{144}Nd$ (ppm)	$^{143}Nd/^{144}Nd$ (ppm)	$\varepsilon_{Nd(t)}$ (ppm)	T_{DM} (Ga)	Age $^{206}Pb/^{238}U$ (Ma)
Castagna unit												
GO 6	175	181	2.79	0.73372	0.71257	35.0	6.9	0.11897	0.51220	–3,19	1.53	547
GO 35	190	156	3.51	0.73557	0.70931	22.1	4.6	0.12454	0.51216	–5,35	1. 69	539
Sila unit												
GO 71	136	154	2.55	0.73010	0.71103	35.5	7.1	0.12132	0.51215	–4,14	1. 65	540
GO 100	125	148	2.44	0.73216	0.71392	35.3	7.1	0.12218	0.51214	–4,57	1. 68	540
Aspromonte unit												
ADR 5	237	132	5.18	0.74968	0.70925	31.9	6.7	0.12705	0.51218	–4,25	1.70	562
ADR 18	187	65	8.30	0.75549	0.69484	26.9	5.5	0.12323	0.51219	–4,65	1.61	526

Sr initial isotopic ratios and ε_{Nd} values are calculated at the U–Pb age obtained on zircon for each sample. CHUR and DM are from De Paolo and Wasserburg (1976)

(Fig. 3a) and peraluminous composition [$1.0 < Al_2O_3/(CaO + Na_2O + K_2O) < 1.9$], with a limited range in SiO_2 contents (68.3–72.9, with the exception of three samples) and a high-K calc-alkaline—shoshonitic signature (Fig. 3b). Chondrite-normalized rare earth patterns (Fig. 3c) are LREE-enriched (La_N/Sm_N = 3.0–3.8), with flat HREE (Gd_N/Yb_N = 1.2–1.9) and a systematically negative Eu anomaly (Eu/Eu* = 0.45–0.58). They closely resemble the REE pattern of the North American Shale Composite (Haskin et al. 1968). Trace element patterns normalized to the primitive mantle are homogeneous (Fig. 3d), with negative anomalies in Ba, Nb, Ta, Sr, P and Ti. $^{87}Sr/^{86}Sr$ initial ratios range from 0.7093 to 0.7139 (with the exception of the anomalously low Sr initial ratio of sample ADR18 at 0.6948); ε_{Nd} values are negative (–3.2 to –5.4) and Nd model ages(T_{DM}) range from 1.5 to 1.7 Ga (Table 4).

Zircon U–Pb geochronology

Five augen gneiss samples were collected from the three units for ion-probe U–Pb dating (Table 5). Zircon crystals from each sample were selected from 50–125 and 125–315 μm fractions extracted from ca. 10 kg of rock, using heavy liquids and a Frantz magnetic separator. Zircons were hand-picked using a binocular microscope and were selected by choosing the clearest, crack- and inclusion-free grains. Selected zircons were mounted in epoxy resin together with fragments of the 91,500 standard zircon (Ontario, Canada; Wiedenbeck et al. 1995). During the measurements the obtained age from the standard zircon ranged between 1062 ± 58 and 1063 ± 12 Ma, in agreement with the reference value of 1062.4 ± 0.4 Ma (Wiedenbeck et al. 1995). Mounts were then polished and gold coated. All zircon grains were inspected by

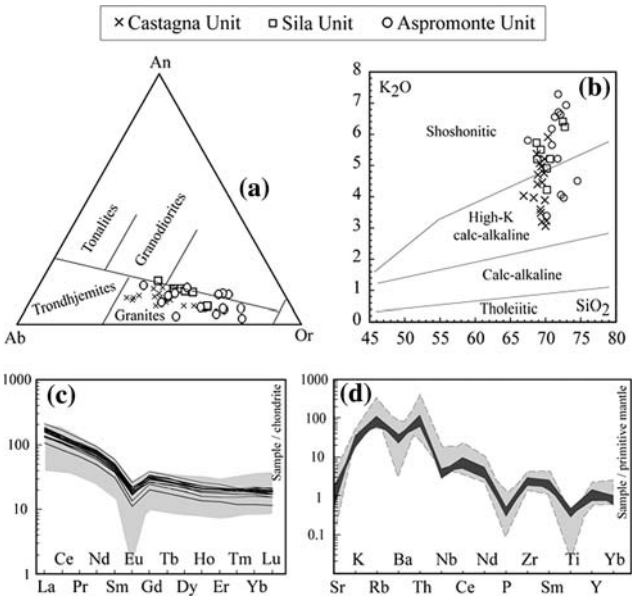


Fig. 3 Major and trace element plots for Calabrian augen gneisses. **a** Ab–An–Or ternary plot; **b** K_2O *versus* SiO_2 plot; **c** REE patterns normalized to chondrite (Mc Donough and Sun 1995) compared with Pan-African granites (*shaded*) from the Tuareg Shield (Azzouni et al. 2003); **d** Multi-element diagram normalized to primitive N-MORB (Sun 1980; Pearce 1983) showing the similarity of Calabrian augen gneisses (*dark shading*) to Pan-African granites (*light shading*) from the Tuareg Shield (Azzouni et al. 2003)

backscattered scanning electron (BSE) and cathodoluminescence (CL) microscopy, before and after ion probe analyses, to investigate their internal microstructures and check the position of the analytical spot with respect to the microstructures.

The selected zircons show moderately elongated prisms (length/width ratio of 3–4), with sharp tips, well-defined and brilliant faces (Figs. 4, 5, 6). Crystals show well preserved euhedral growth zones, with unperturbed oscillatory zoning typical of magmatic growth (Hanchar and Miller 1993). Magmatic zoning develops either in continuity with euhedral cores, or surrounds resorbed rounded cores. Some zircon grains show strongly luminescent cores or growth bands. They may be considered as recrystallized domains resulting from zoning controlled alteration (Vavra et al. 1996, 1999). Zircon grains of sample GO100, from the highest grade zone, show a 10 μm thick luminescent outer rim. Attempts to determine its isotopic composition were unsuccessful.

U–Pb isotopic compositions were determined in situ using the CRPG-CNRS Cameca IMS-1270 ion microprobe (Nancy, France). Primary O^{2-} ion beam was accelerated at 13 kV with an intensity that ranged between 5 and 20 nA, and focused on a 20–25 μm diameter area, providing a mean secondary ions yield of 25cps/nA/ppm. Each spot was analysed for 18 min, after a presputterring of 2 min. An empirical relationship between UO^+/U^+ and Pb^+/U^+ was defined from all the measurements performed on the standard parts of each sample mount in order to determine the relative sensitivity factor for Pb and U used for samples (Compston et al. 1984). Correction for common lead was made by measuring the ^{204}Pb amount. The common lead composition was calculated at $^{207}Pb/^{206}Pb$ measured ages, using Stacey and Kramers model (1975). The $^{206}Pb/^{204}Pb$ ratios range in most case from 3,000 to more than 50,000, and thus the common Pb composition chosen for correction is not highly critical. Further information on instrumental conditions and data reduction procedures are found in Deloule et al. (2002). Isotopic data with analytical uncertainties and calculated ages are given in Table 6. Errors include the analytical statistical error, the error associated with the common lead correction and the systematic error associated with the U/Pb calibration procedure (Deloule et al. 2002). Concordia diagrams (Figs. 4, 5, 6) and discordia lines were constructed using the Isoplot program (Ludwig 2003). In the forthcoming paragraphs, we use $^{206}Pb/^{238}U$ ages for concordant data, rather than $^{207}Pb/^{235}U$ ages, which are more sensitive to

Table 5 Location of samples selected for zircon U–Pb dating

Unit	Sample	Site	Coordinates		Rock type
			Latitude	Longitude	
Castagna	GO6	Tiriolo	38°57′31″	16°31′31″	Lower-medium grade, weakly deformed, biotite augen gneisses, with limited alpine greenschist facies retrogression
	GO35	Taverna	39° 01′28″	16° 35′15″	
Sila	GO100	Montepaone	38° 43′38″	16° 28′56″	Amphibolite facies, partially melted biotite-garnet augen gneiss, without significant alpine metamorphic overprint
Aspromonte	ADR5	Palizzi	37° 56′08″	15° 58′43″	Weakly deformed, amphibolite facies biotite augen gneisses, with limited alpine reworking
	ADR18	Roccaforte del Greco	38° 02′40″	15° 54′06″	

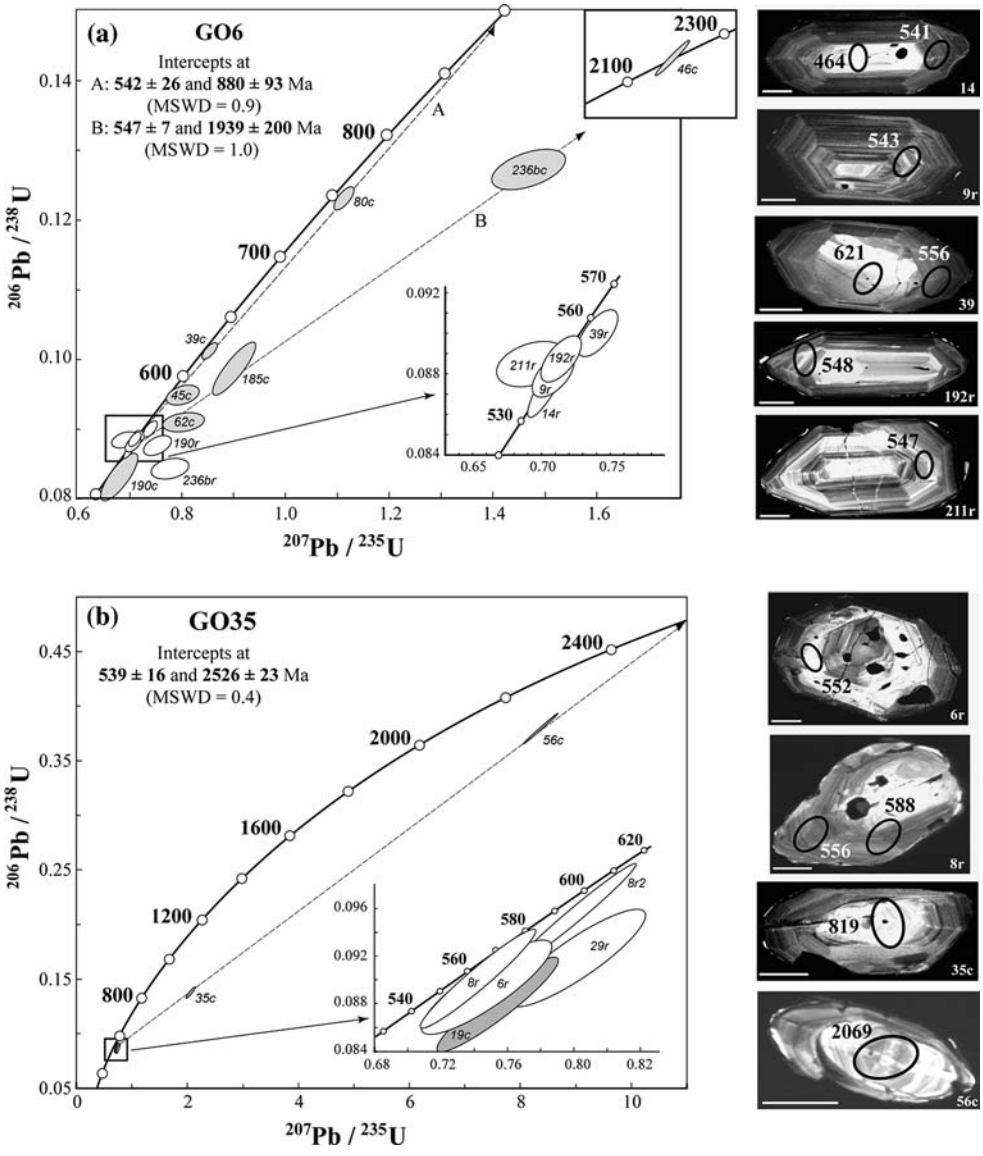


Fig. 4 U–Pb Concordia diagrams for the samples GO6 (**a**) and GO35 (**b**) from the augen gneisses of the Castagna Unit and cathodoluminescence images of some zircons with the analyzed spots; ellipses represent 2σ, in grey core analyses and in white rim analyses; values are $^{206}Pb/^{238}U$ ages. Scale bar for zircons: 50 μm

common lead contribution (the ^{207}Pb ion signal is about ten times lower than the ^{206}Pb ion signal). The discordant data were considered on the concordia diagrams to obtain the possible discordia lines.

Castagna unit

Among the zircon grains from sample GO6 (Fig. 4a), five rims (9r, 14r, 39r, 192r, 211r) give concordant data within error, with $^{206}Pb/^{238}U$ ages at 543 ± 4, 541 ± 7, 556 ± 5, 548 ± 5 and 547 ± 4 Ma. Two cores (46c, 14c) yield concordant ages at 2216 ± 56 and 464 ± 4 Ma (the latter is an age significantly younger than the mean age of the rims). The other data are discordant. Regression of zircon data 9r, 14r, 39r, 45c, 62c, 185c 192r, 211r and 236bc gives a discordia line with lower and upper intercepts at 547 ± 7 and 1939 ± 200 Ma (MSWD = 1.05), respectively. Regression of data 9r, 14r, 39c, 39r, 80c, 192r and 211r gives a discordia line with lower and upper intercepts at 542 ± 26 and 880 ± 93 Ma (MSWD = 0.86).

Age data for rims and cores of zircons from sample GO35 are discordant (Fig. 4b), with the exception of two rims (6r, 8r) with sub-concordant ages at 552 ± 16 and 556 ± 16 Ma. Sub-concordant analysis 8r2 has not been taken into account as it appears to be a core-rim mixture. The discordia line through six data (6r, 8r, 19c, 29r, 35c, 56c) gives lower and upper intercepts at 539 ± 16 and 2526 ± 23 Ma (MSWD = 0.42), respectively.

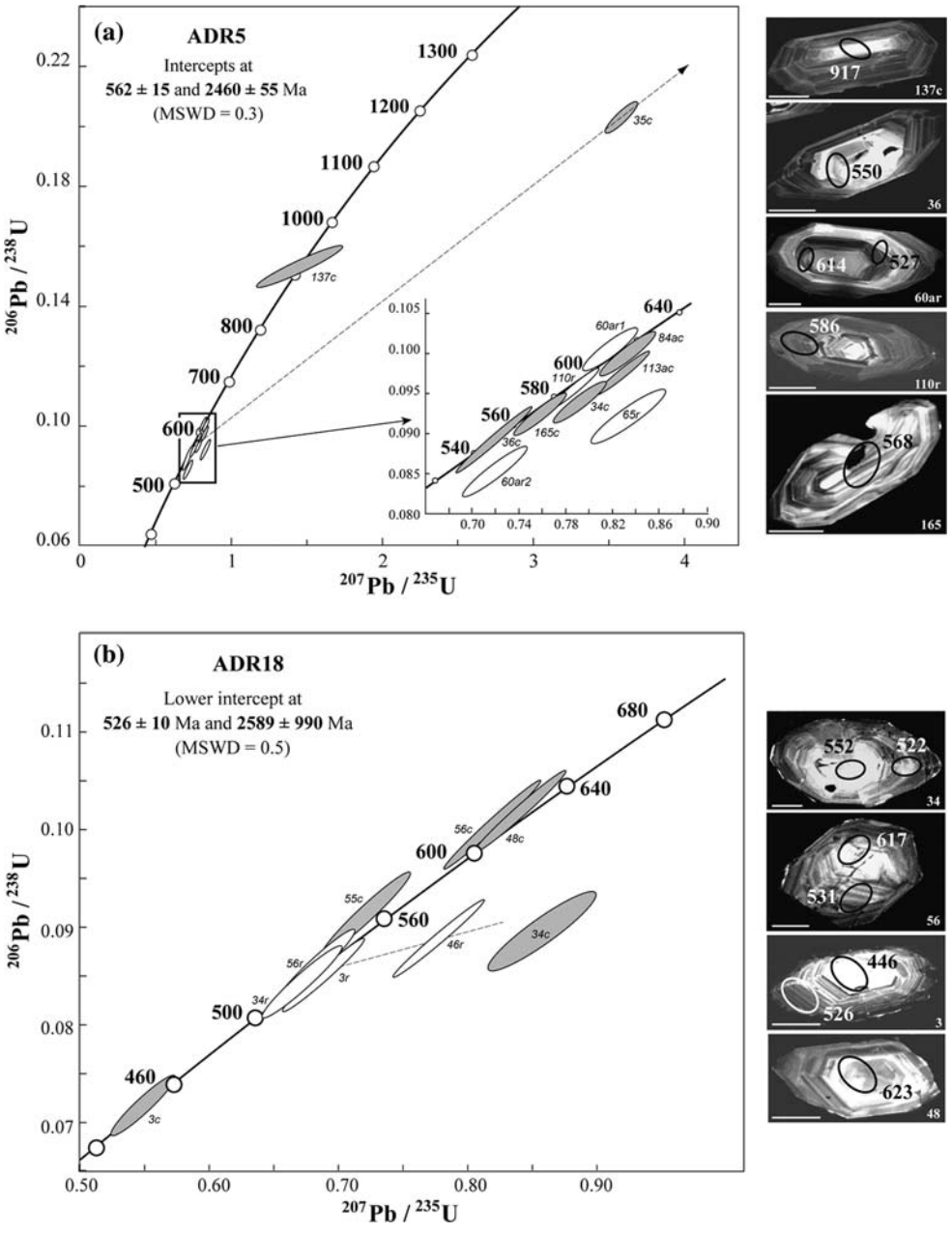


Fig. 5 U–Pb Concordia diagrams for the samples ADR5 (**a**) and ADR18 (**b**) from the augen gneisses of the Aspromonte Unit and cathodoluminescence images of some zircons with the analyzed spots; ellipses represent 2σ,in grey core analyses and in white rim analyses; values are $^{206}Pb/^{238}U$ ages. Scale bar for zircons: 50 μm

Aspromonte unit

In sample ADR5 (Fig. 5a), four grains (36c, 110r, 165c, 137c) yield concordant ages at 550 ± 16, 568 ± 10, 586 ± 10 and 917 ± 26 Ma. Slightly discordant ages 113ac, 60ar1 and 60ar2 are probably without significance because they correspond to core-rim mixtures. The discordia line through five data (34c, 35c, 36c and 165c) gives lower and upper intercepts at 562 ± 15 and 2460 ± 55 Ma (MSWD = 0.31).

In sample ADR18 (Fig. 5b), three concordant rims (3r, 34r, 56r) give ages at 526 ± 15, 522 ± 15 and 531 ± 15 Ma. Two cores (3c and 48c) give concordant ages at 446 ± 13 and 623 ± 18 Ma. Analysis 56c yielding concordant age at 617 ± 17 Ma appears to correspond to core-rim mixture and will not be considered further. Regression of data 3r, 34r, 46r and 56r gives a discordia line with a lower and upper intercepts at 526 ± 10 and 2589 ± 990 Ma (MSWD = 0.52).

Sila unit

In zircons from sample GO100 (Fig. 6), five analyses (5r, 33br, 114r, 153c and 274r) give concordant ages at

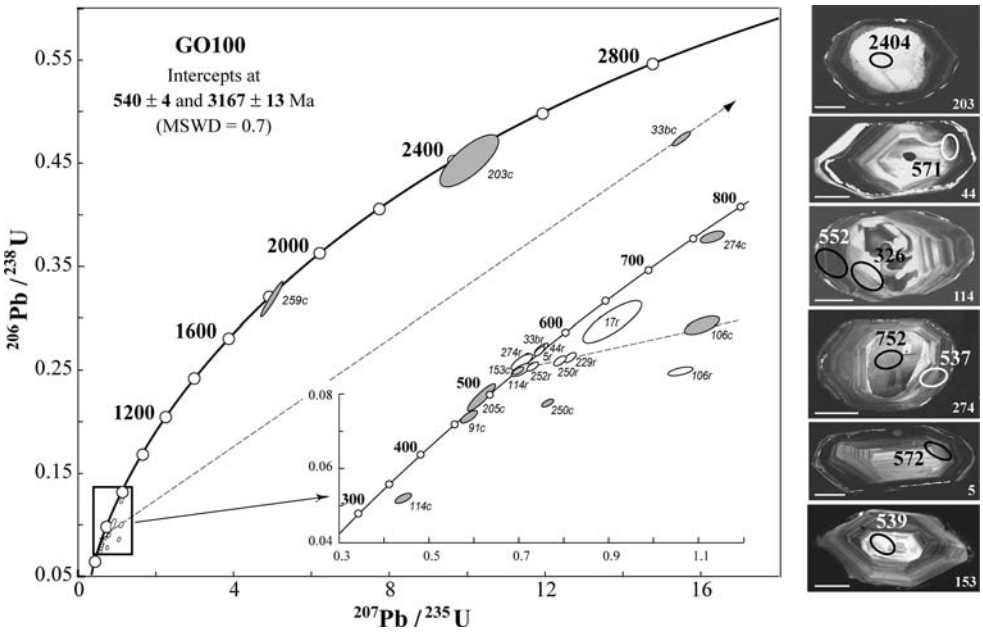


Fig. 6 U–Pb Concordia diagram for the sample GO100 from the augen gneisses of the Sila Unit and cathodoluminescence images of some zircons with the analyzed spots; ellipses represent 2σ,in grey core analyses and in white rim analyses; values are $^{206}Pb/^{238}U$ ages. Scale bar for zircons: 50 μm

572 ± 6, 575 ± 4, 552 ± 9, 539 ± 7 and 537 ± 4 Ma. Rim analysis 44r has not been taken into account as it corresponds to a core-rim mixture. Two cores (203c, 259c) give concordant ages at 2404 ± 92 and 1760 ± 46 Ma. Cores 91c and 205c give concordant ages (462 ± 7, 494 ± 14 Ma) significantly younger than the rims. All other data are discordant. Regression of analyses 33bc, 106c, 114r, 153c, 229r, 250r, 252r and 274r yield a discordia line with lower and upper intercepts at 540 ± 4 and 3167 ± 13 Ma (MSWD = 0.74).

Discussion

On the whole, geochemical data show that the augen gneisses from Calabria derive from high-K porphyritic granite protoliths. Their Sr initial ratios of 0.7093–0.7140 and $\varepsilon_{Nd(t)}$ values of –3.2 to –5.4 ranging from those of metabasites to those of metasediments of the lower crustal portion of the Sila Unit in northern Serre (e.g. Caggianelli et al. 1991) suggest an important crustal contribution in the genesis of protoliths. The crustal contribution is supported by the presence of abundant inherited cores in zircons, which give Neoproterozoic, Palaeoproterozoic and Archaean ages. The multi-element plot (Fig. 3a, b) points to post-collisional high-K calc-alkaline magmatism, with important crustal involvement (Barbarin 1998). These characteristics are close to those reported for Pan-African granites of the West African craton (e.g Gasquet et al. 2005).

Geochronological data

Analyses on individual zircons from the five orthogneiss samples define several age groups, irrespective of the tectonic units wherein they were collected. They reflect the heterogeneity of the zircon populations as observed in polyphase domains.

Magmatic rims and two zircon grains give Latest Precambrian to Early Cambrian concordant $^{206}Pb/^{238}U$ ages, which range for most of them, from 522 ± 15 to 556 ± 16 Ma, with the exception of four data ranging from 568 ± 10 to 586 ± 10 Ma.

The lower intercepts of discordia lines relative to the five analyzed samples are 539 ± 16, 542 ± 26 and 547 ± 7 Ma (Castagna Unit), 526 ± 10 and 562 ± 15 Ma (Aspromonte Unit) and 540 ± 4 Ma (Sila Unit). These ages are consistent with the single data of each sample and corroborate that the emplacement age of the protolith of the augen gneisses is Latest Precambrian to Early Cambrian.

Neoproterozoic and Palaeoproterozoic concordant ages (623 ± 18, 917 ± 26, 1760 ± 46, 2404 ± 92 and 2216 ± 56 Ma) obtained from zircon cores are consistent with the upper intercept values (880 ± 93, 1939 ± 200, 2460 ± 55 and 2526 ± 23 Ma). An Archaean age is given by the upper intercept of the discordia line defined by GO100 (3167 ± 13 Ma). All these ages likely represent ancient components inherited from the source of the protolith of the augen gneisses.

Ordovician concordant and sub-concordant ages (446 ± 13, 462 ± 7, 464 ± 4 and 494 ± 14 Ma) are

Table 6 Zircon U–Pb isotopic data for samples of augen gneiss from Calabria

Anal. Spot	$^{206}Pb^{204}Pb$ measured	Concentrations (ppm)			Corrected ratios						Ages						
		Pb	U	Th	$^{206}Pb/^{238}U$	±σ	$^{207}Pb/^{235}U$	±σ	$^{207}Pb/^{206}Pb$	±σ	$^{207}Pb/^{206}Pb$	±σ	$^{206}Pb/^{238}U$	±σ	$^{207}Pb/^{235}U$	±σ	Conc. %
GO6 (Castagna Unit)																	
9r	7692	27	356	72	0.08795	0.00072	0.70849	0.00989	0.05842	0.01132	545. 6	24.4	543.4	4.3	543.9	5.9	–
14c	20000	72	1123	21	0.07470	0.00064	0.58467	0.00572	0.05677	0.00479	482. 6	10.6	464.4	3.8	467.5	3.7	96.2
14r	25000	112	1484	44	0.08752	0.00110	0.70512	0.01005	0.05843	0. 00681	545.9	14.8	540.9	6.5	541.8	6.0	99.1
39c	16667	27	307	201	0.10108	0.00080	0.85253	0.00947	0.06117	0.00775	645. 3	16.6	620.7	4.7	626.0	5.2	96.2
39r	16667	29	369	74	0.09002	0.00075	0.74089	0.00954	0.05969	0.00980	592. 5	21.10	555.6	4.5	562.9	5.6	93.8
45c	2941	14	163	181	0.09490	0.00091	0.80431	0.02061	0.06147	0.02378	655.6	50.2	584.5	5.3	599.3	11.5	89.2
46c	16667	38	107	95	0.41030	0.01238	7.85431	0.23920	0.13848	0.00418	2212. 7	6.9	2216.3	56.3	2214.5	27.1	100.2
62c	1250	14	171	118	0.09101	0.00086	0.80565	0.02657	0.06420	0.03159	748. 5	65.4	561.5	5.1	600.0	14.8	75.0
80c	14286	23	222	223	0.12306	0.00103	1.11504	0.01264	0.06572	0.00763	797. 3	15.9	748.2	5.9	760.6	6.1	93.8
185c	4348	6	74	45	0.09879	0.00251	0.90396	0.02686	0.06636	0.01542	817. 9	31.9	607.3	14.7	653.8	14.2	74.3
190c	1493	5	69	14	0.08309	0.01970	0.68137	0.02843	0.05947	0.02049	584. 5	39.9	514.6	9.7	527.6	11.6	88.1
190r	3030	22	289	227	0.08770	0.00089	0.75517	0.01774	0.06245	0.02116	689. 6	44.5	541.9	5.3	571.2	10.2	78.6
192r	10000	26	340	62	0.08875	0.00076	0.71440	0.00954	0.05838	0.01023	544. 1	22.2	548.1	4.5	547.4	5.6	100.7
211r	3571	30	392	84	0.08848	0.00074	0.69314	0.01698	0.05682	0.02301	484. 4	50.0	546.6	4.4	534.7	10.1	112.8
236br	50000	14	197	119	0.08429	0.00096	0.77680	0.02421	0.06684	0. 02902	832.8	59.4	521.7	5.7	583.7	13.7	62.6
236bc	847	76	692	183	0.12722	0.00187	1.47177	0.04648	0.08390	0. 02797	1291	53.5	772.0	10.7	918.9	18.9	59.8
GO35 (Castagna Unit)																	
6r	4762	21	272	54	0.08935	0.00266	0.74658	0.02588	0.06060	0.01784	625. 0	35.7	551.7	15.7	566.2	14.9	88.3
8r	8333	24	305	111	0.09005	0.00271	0.74141	0.02315	0.05971	0.00843	593. 2	16.4	555.8	16.0	563.2	13.4	93.7
8r2	25000	37	455	99	0.09550	0.00284	0.80033	0.02421	0.06078	0.00540	631. 5	11.1	587.9	16.7	597.0	13.6	93.1
19c	2857	16	216	160	0.08796	0.00264	0.75350	0.02422	0.06213	0.01164	678. 6	22.1	543.5	15.6	570.3	13.9	80.1
29r	33333	31	388	71	0.09181	0.00274	0.80088	0.02716	0.06327	0.01608	717. 2	33.9	566.2	16.2	597.3	15.2	78.9
35c	3571	24	207	110	0.13546	0.00424	2.00778	0.06587	0.10750	0.00977	1757. 6	16.7	818.9	24.0	1118.1	22.0	46.6
56c	25000	103	316	389	0.37843	0.01116	8.36209	0.24748	0.16026	0. 00237	2458.4	3.8	2068.9	52.0	2271.1	26.5	84.2
GO100 (Sila Unit)																	
5r	25000	83	1040	102	0.09286	0.00109	0.75181	0.00959	0.05872	0.00496	556. 7	10.8	572.4	6.4	569.3	5.6	102.8
17r	33333	85	984	102	0.10046	0.00388	0.91163	0.04379	0.06582	0.02863	800. 5	59.8	617.1	22.7	657.9	23	77.1
33br	33333	74	928	98	0.09328	0.00070	0.74878	0.00615	0.05822	0.00339	538. 0	7.4	574.9	4.1	567.5	3.6	106.9
33bc	100000	90	220	184	0.47421	0.00426	15.4948	0.14973	0.23698	0. 00357	3099.8	5.7	2502.0	18.6	2846.2	9.2	80.7
44r	50000	146	1832	118	0.09260	0.00071	0.74818	0.00621	0.05860	0. 00325	552.3	7.1	570.9	4.2	567.2	3.6	103.4
91c	6667	16	244	214	0.07427	0.00109	0.59019	0.01211	0.05764	0.01430	515. 9	31.1	461.8	6.6	470.9	7.7	89.5
106c	5556	13	158	111	0.09929	0.00149	1.11102	0.02555	0.08115	0. 01739	1225.2	33.8	610.3	8.8	758.7	12.2	49.8
106r	14286	31	416	49	0.08682	0.00084	1.06278	0.01880	0.08878	0. 01478	1399.5	28.1	536.7	5.0	735.2	9.2	38.3
114c	1613	19	433	61	0.05184	0.00086	0.44384	0.01149	0.06209	0.01994	677. 4	42.1	325.8	5.2	372.9	8.1	48.1
114r	25000	77	1004	91	0.08942	0.00146	0.70953	0.01540	0.05755	0. 01431	512.7	31.1	552.1	8.6	544.5	9.1	107.7
153c	5556	9	122	79	0.08718	0.00126	0.70687	0.01388	0.05881	0.01335	560. 0	28.8	538.8	7.4	542.9	8.2	96.2
203c	25000	27	68	69	0.45207	0.02078	10.2513	0.57222	0.16446	0.03166	2502. 1	52.3	2404.4	91.6	2457.7	50.4	96.1
GO100 (Sila Unit)																	
205c	7692	12	177	92	0.07966	0.00237	0.61903	0.02063	0.05636	0.01501	466. 5	29.4	494.1	14.1	489.2	12.9	105.9
229r	20000	64	822	69	0.09053	0.00072	0.81709	0.00914	0.06546	0.00784	789. 1	16.4	558.7	4.3	606.4	5.1	70.8
250c	20000	25	374	228	0.07811	0.00067	0.76618	0.00821	0.07114	0. 00644	961.6	13.1	484.8	4.0	577.6	4.7	50.4
250r	16667	41	527	69	0.08959	0.00070	0.79368	0.00903	0.06425	0.00825	749. 9	17.3	553.1	4.2	593.3	5.1	73.8

Table 6 continued

Anal. Spot	$^{206}Pb^{204}Pb$ measured	Concentrations (ppm)			Corrected ratios						Ages						
		Pb	U	Th	$^{206}Pb/^{238}U$	$\pm\sigma$	$^{207}Pb/^{235}U$	$\pm\sigma$	$^{207}Pb/^{206}Pb$	$\pm\sigma$	$^{207}Pb/^{206}Pb$	$\pm\sigma$	$^{206}Pb/^{238}U$	$\pm\sigma$	$^{207}Pb/^{235}U$	$\pm\sigma$	Conc. %
252r	100000	29	378	43	0.08819	0.00074	0.73257	0.00791	0.06025	0. 00680	612.5	14.6	544.8	4.4	558.1	4.6	88.9
274r	16667	34	453	100	0.08692	0.00065	0.70117	0.00767	0.05851	0. 00796	548.8	17.3	537.3	3.9	539.5	4.6	97.9
274c	7692	14	135	100	0.12372	0.00104	1.13573	0.01723	0.06658	0. 012633	824.6	26.2	751.9	6.0	770.5	8.2	91.2
259c	100000	91	339	209	0.31386	0.00936	5.01279	0.15009	0.11584	0. 00253	1892.9	4.5	1759.7	45.8	1821.5	25.0	93.0
ADR5 (Aspromonte Unit)																	
34c	14286	8	94	23	0.09359	0.01781	0.79279	0.01902	0.06144	0.00668	654. 6	13.0	576.7	9.8	592.8	8.5	88.1
35c	33333	21	119	18	0.20263	0.01787	3.58641	0.01990	0.12837	0.00878	2075. 7	15.2	1189.5	19.4	1546.5	15.7	57.3
36c	12500	18	241	111	0.08906	0.00263	0.71913	0.02147	0.05856	0.00408	550. 8	8.3	550.0	15.6	550.2	12.6	99.9
60ar1	25000	11	132	11	0.09985	0.01740	0.81844	0.01884	0.05945	0. 00723	583.6	–	613.5	10.2	607.2	8.6	105.1
60ar2	4762	4	54	6	0.08517	0.02381	0.72021	0.02543	0.06133	0.00894	650. 9	18.1	526.9	12.0	550.8	10.8	80.9
65r	33333	10	128	6	0.09175	0.02333	0.83395	0.02547	0.06592	0.01022	–	–	565.9	12.6	615.8	11.7	–
84ac	14286	5	63	15	0.09935	0.01804	0.83375	0.01904	0.06086	0.00611	634. 4	12.3	610.6	10.5	615.7	8.8	96.2
110r	50000	12	151	11	0.09515	0.01726	0.78819	0.01792	0.06008	0.00482	606. 4	10.3	585.9	9.7	590.1	8.0	96.6
113ac	14286	9	114	22	0.09700	0.01744	0.82953	0.01791	0.06203	0.00408	674. 9	8.1	596.8	9.9	613.4	8.2	88.4
137c	820	6	43	9	0.15277	0.03033	1.45835	0.13085	0.06924	0.12728	906. 0	237	916.5	25.9	913.3	75.9	101.2
165c	5000	8	102	6	0.09213	0.01920	0.75986	0.02017	0.05982	0.00619	596. 9	12.0	568.1	10.4	573.9	8.8	95.2
ADR18 (Aspromonte Unit)																	
3c	7143	15	246	161	0.07166	0.00213	0.54840	0.01718	0.05550	0.00991	432. 5	20.2	446.2	12.8	443.9	11.2	103.2
3r	14286	33	458	80	0.08509	0.00252	0.68881	0.02082	0.05871	0.00599	556. 5	–	526.4	15.0	532.1	12.4	94.6
34c	16667	22	283	114	0.08937	0.00266	0.85792	0.02756	0.06963	0.01208	917.3	24. 4	551.8	15.7	629.0	15.0	60.2
34r	11111	27	373	224	0.08427	0.00249	0.67000	0.02030	0.05766	0.00660	517. 0	13.7	521.6	14.8	520.7	12.3	100.9
46r	16667	46	605	63	0.08874	0.00264	0.77778	0.02345	0.06357	0.00471	–	–	548.1	15.6	584.2	13.3	–
48c	14286	34	388	234	0.10150	0.00300	0.83880	0.02519	0.05994	0.00511	601. 4	10.4	623.2	17.6	618.5	13.8	103.6
55c	11111	29	374	67	0.09158	0.00273	0.72319	0.02225	0.05727	0.00746	502. 1	15.6	564.9	16.1	552.5	13.0	112.5
56c	8333	56	651	71	0.10038	0.00298	0.82018	0.02461	0.05926	0.00441	576. 6	–	616.7	17.4	608.2	13.6	107.0
56r	20000	39	533	162	0.08590	0.00255	0.68217	0.02008	0.05760	0.00721	514. 4	15.2	531.3	15.1	528.1	12.5	103.3

obtained from cores of zircons from Castagna, Sila and Aspromonte Units. These cores display irregular and patchy microstructures and some of them are strongly luminescent. These ages, significantly younger than the rims, are considered as recrystallized domains (see Vavra et al. 1996, 1999), which could be related to an Ordovician tectonometamorphic activity, as formerly suggested by Schenk (1990), or to an hydrothermal episode (Hoskin and Schaltegger 2003). In analogous times is further suggested an important magmatic activity producing porphyroids known in NE Sicily at ca. 450–480 Ma (Table 1; Trombetta et al. 2004). Nevertheless, it cannot be excluded that these ages might result from rejuvenation due to the opening of U–Pb radiogenic system with partial loss of Pb during the Variscan metamorphism.

Lastly, the thin, unzoned, luminescent outer rims of zircons from sample GO100 collected in the high-grade domain are tentatively attributed to the Variscan metamorphism.

Geodynamic implications

Zircon U–Pb data show that the Calabrian augen gneisses are distinct from the porphyroids of the Peloritani Mountains in NE Sicily, which are Late Ordovician in age (452–456 Ma in Trombetta et al. 2004). They are also older than the granitic orthogneisses from Sardinia, Petite Kabylie and eastern Pyrenees, which are also related to an Ordovician magmatic activity (Table 1). Our results explain the range of ages from 549 ± 4 to 622 ± 120 Ma, previously published by Senesi (1999) and Schenk and Todt (1989), the former being close to our mean age of emplacement, the latter corresponding more likely to inheritance. These data allow that the Latest Precambrian to Early Cambrian emplacement age of the magmatic protolith, can be extended to the whole Calabrian orthogneisses and show that the granitoids emplaced coevally, within uncertainties, with the protoliths of the mafic metamorphic rocks dated at 553 ± 27 Ma (Schenk 1980) in the Serre. The Calabrian augen gneisses, therefore, belong to the group *i* (Table 1) present throughout the central European Variscides. Should we see regularity in the distribution of orthogneiss ages? Indeed, the Lower–Middle Ordovician ages seem to occur mainly towards the west (i.e. towards the zone of rifting), whereas the older orthogneisses seem to be located mainly in the east area from Calabria to the Bohemian Massif, representing the older continental domains (von Raumer et al. 2002).

The Calabria–Peloritani domain is considered as an ''exotic terrane'' belonging to the Alboran micro-continent (Andrieux et al. 1971). Paleogeographic reconstructions in Precambrian times (e.g. Stampfli et al. 2002; von Raumer et al. 2002, 2003) indicate that this microplate was one of the peri-Gondwana terranes on the northern margin of the supercontinent Gondwana showing analogies with Cadomian terranes. As discussed below, our results not only are consistent with this model, but also suggest that the Alboran microplate might have been a piece of the northern edge of the West-African craton.

The contribution of an old continental crust in the genesis of the protolith of the Calabrian augen gneisses appears from the zircon age data showing Archaean, Palaeoproterozoic and Pan-African inheritance, and from the Sm–Nd model ages ranging from 1.5 to 1.7 Ga (Table 4). The presence of an older craton submitted to erosion is also supported by the age recorded in metasediments of the Sila Unit in the Serre, whose zircons produced ages at 2.5, 2.3, 2.0 and 1.9 Ga (Schenk and Todt 1989; Schenk 1990). Analogies with orthogneisses of Central and Eastern Europe are also striking, where Archaean, Palaeoproterozoic and Pan-African ages are commonly recorded in zircons. Similar age groups are also known in zircons of metasedimentary sequences associated with orthogneisses (3.8–3.1, 2.9–2.6, 2.4–2.1, 2.0–1.7, 0.65–0.57 Ga) as for example in northern France, the Channel Islands, Bavaria, Eastern Erzgebirge, Alps, Massif Central and NW Iberia (Gebauer et al. 1989; Schaltegger and Gebauer 1999; Fernandez-Suarez et al. 2000; Tichomirowa et al. 2001; Samson et al. 2005). This group of ages and the lack of Mesoproterozoic ages, typically absent in the Cadomian terranes (Cahen et al. 1984) and related to the Avalonian terranes and the Grenville belts (Mallard and Rogers 1997; Murphy et al 2006), suggest that the source material of the magmatic protolith of Calabrian augen gneisses could be derived from the West African Craton (Samson et al. 2005).

The ages obtained from the Calabrian augen gneisses share similarities with the pattern of ages at the northern edge of the West African Craton, especially in Morocco (Thomas et al. 2002; Walsh et al. 2002; Acef et al. 2003). Gasquet et al. (2005) show that the Pan-African magmatism in the Anti-Atlas domain can be described into three main stages: ocean opening and subduction (690–790 Ma, with peaks at 790 and 690 Ma); ocean closure and arc-continent collision (605–690 Ma, with peaks at 660 and 615 Ma); and transition to a passive continental margin coupled with extension and development of foreland basins (530–605 Ma, with peaks at 590, 550 and 530 Ma). Our age data ranging from 562 ± 15 to 526 ± 10 Ma are in close agreement with the

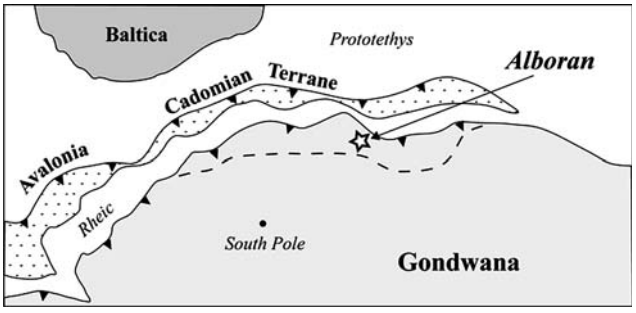


Fig. 7 Possible paleogeographic reconstruction of the Alboran microplate position on the northern Gondwana margin in Pre-Cambrian time (modified after: von Raumer et al. 2002, 2003; Giacomini et al. 2005)

Pan-African magmatism in northern Africa. Similar age patterns are also reported in the Tuareg Shield (Azzouni-Sekkal et al. 2003). The age range recorded in the West African Craton in Mauritania (Reguibat Rise; Lahondére et al. 2004) is also in good agreement with the inherited ages: Mesoarchaean (>3.05 Ga), Eobirimian (>2.15 Ga) and Neobirimian (ca. 2.0 Ga). Emplacement ages at 1.75 Ga are also recorded in Moroccan Anti-Atlas (Gasquet et al. 2004, 2005).

The analogy with these terranes is strongly reinforced by the similarity of the geochemical signatures of the protoliths of the Calabrian augen gneisses compared to the post-collisional Pan-African products at the northern margin of the West African Craton. This period (605–530 Ma) corresponds to a change from an active (compressive–transtensive) to a passive (extensional) margin, with voluminous high-K calc-alkaline plutonism and volcanism showing mantellic and crustal signatures (e.g. Gasquet et al. 2005). Even though any attempt to replace the Calabria–Peloritani domain within the framework of the Pan-African of North Africa remains speculative (Fig. 7), the similarity of the geochronological and geochemical features of the Calabrian augen gneisses with the Pan-African plutonism speaks in favour of a common origin.

Conclusion

Ion-probe U–Pb analyses of individual zircon grains allow the emplacement age of the magmatic protolith of the Calabrian augen gneisses (Sila, Serre and Aspromonte) to be estimated between 562 ± 15 and 526 ± 10 Ma. The older Archaean to Neoproterozoic ages are considered to represent the contribution of inherited components representing source (or possibly exotic) materials. The Calabrian orthogneisses are more akin to the calc-alkaline orthogneisses of the central and eastern European Variscides and to the high-K calc-alkaline granitoids of North Africa rather than to those of Western Europe, which are Lower Ordovician. The emplacement age, geochemical affinity and inheritance show that the granitic protolith of the Calabrian orthogneisses belong to the post-collisional phase of the Pan-African orogeny. These results reinforce the idea that the Calabria–Peloritani ''terrane'' and the Alboran microplate were a piece of the northern margin of the West African craton.

Acknowledgments Thanks to M. Champenois, C. Rollion-Bard and D. Mangin for technical development of the ion-probe facilities. W. H. Dullo, F. Corfu, D. Gasquet, J. F. von Raumer and A. Rottura are gratefully acknowledged for their constructive criticisms. This study benefited from financial support from CRPG-CNRS of Nancy and University of Bari.

References

Abati J, Dunning GR, Arenas R, Diaz Garcia F, Gonzales Cuadra P, Martinez Catalan JR, Andonaegui P (1999) Early Ordovician orogenic event in Galicia (NW Spain): evidence from U–Pb ages in the uppermost unit of the Ordenes Complex. Earth Planet Sci Lett 165:213–228

Acef K, Liégeois JP, Ouabadi A, Latouche L (2003) The Anfeg post-collisional Pan-African high-K calc-alkaline batholith (Central Hoggar, Algeria), result of the LATEA microcontinent metacratonisation. J Afr Earth Sci 37:295–311

Acquafredda P, Laviano R, Di Lecce V (1985) Manuale teorico pratico su ''Analisi chimiche per Fluorescenza RX ed elaborazione al calcolatore dei dati per la correzione degli effetti di matrice''. Relazione interna, Dipartimento Geomineralogico, University of Bari, pp 1–38

Acquafredda P, Lorenzoni S, Zanettin Lorenzoni E (1994) Paleozoic sequences and evolution of the Calabrian–Peloritani Arc (Southern Italy). Terra Nova 6:582–594

Amodio Morelli L, Bonardi G, Colonna V, Dietrich D, Giunta G, Ippolito F, Liguori V, Lorenzoni S, Paglionico A, Perrone V, Piccarreta G, Russo M, Scandone P, Zanettin Lorenzoni E, Zuppetta A (1976) L'arco Calabro-Peloritano nell'orogene Appenninico-Maghrebide. Mem Soc Geol Ital 17:1–60

Andrieux J, Fontbote JM, Mattauer M (1971) Sur un modéle explicatif de l'Arc de Gibraltar. Earth Planet Sci Lett 12:191–198

Ayalew D, Barbey P, Marty B, Reisberg L, Yirgu G, Pik R (2002) Source, genesis and timing of giant ignimbrite deposits associated with Ethiopian continental flood basalts. Geochim Cosmochim Acta 66:1429–1448

Azzouni-Sekkal A, Liégeois JP, Bechiri-Benmerzoug F, Belaidi-Zinet S, Bonin B (2003) The ''Taourirt'' magmatic province, a marker of the closing stage of the Pan-African orogeny in the Tuareg Shield: review of available data and Sr-Nd isotope evidence. J Afr Earth Sci 37:31–350

Ballévre M, Capdevila R, Guerrot C, Peucat JJ (2002) Discovery of an alkaline orthogneiss in the eclogite-bearing Cellier unit (Champtoceaux Complex, Armorican Massif): a new witness of the Ordovician rifting. C R Geosci 334:303–311

Barbarin B (1998) A review of the relationships between granitoid types, their origins and their geodynamic environments. Lithos 46:605–626

Bonardi G, Compagnoni R, Messina A, Perrone V (1984) Riequilibrazioni metamorfiche di probabile età Alpina dell Unità dell'Aspromonte—Arco Calabro—Peloritano. Rend Soc Ital Mineral Petrol 39:613–628

Bonardi G, Giunta G, Messina A, Perrone V, Russo M (1996) The Calabria–Peloritani Arc. In: Field trip guidebook. 6th field meeting IGCP project n. 276, the Calabria–Peloritani Arc and its correlation with Northern Africa and Southern Europe, vol 6. IGCP, 276, Newsletter, pp 1–80

Bonardi G, Cavazza W, Perrone V, Rossi S (2001) Calabria–Peloritani terrane and northern Ionian Sea. In: Vai GB, Martini IP (eds) Anatomy of an Orogen: the Apennines and adjacent Mediterranean Basins. Kluwer, Dordrecht, pp 287–306

Bouillin JP (1984) Nouvelle interprétation de la liaison Apennin-Maghrébides en Calabre: conséquences sur la paléogéographie téthysienne entre Gibraltar et les Alpes. Rev Géogr Phys Géol Dyn 25:321–338

Bouillin JP, Durand-Delga M, Olivier P (1986) Betic-Rifian and Tyrrhenian arcs: distinctive features, genesis and development stages. In Wezel FC (ed) The origin of arcs. Elsevier, Amsterdam, pp 281–304

Bussy F, Derron MH, Jacquod J, Sartori M, Thelin P (1996) The 500 Ma old Thyon metagranite: a new A-type granite occurrence in the western Penninic Alps (Wallis, Switzerland). Eur J Mineral 8:565–575

Caggianelli A, Del Moro A, Paglionico A, Piccarreta G, Pinarelli L, Rottura A (1991) Lower crustal granite genesis connected with chemical fractionation in the continental crust of Calabria (Southern Italy). Eur J Mineral 3:159–180

Caggianelli A, Prosser G, Del Moro A (2000) Cooling and exhumation history of deep-seated and shallow level, late Hercynian granitoids from Calabria. Geol J 35:33–42

Cahen L, Snelling NJ, Delhal J, Vail JR (1984) The Geochronology and evolution of Africa. Clarendon Press, Oxford

Carignan J, Hild P, Mévelle G, Morel J, Yeghicheyan D (2001) Routine analyses of trace elements in geological samples using flow injection and low pressure on-line liquid chromatography coupled to ICP-MS: a study of reference materials BR, DR-N, UB-N, AN-G and GH. Geostand Newsl 25:187–198

Chen F, Hegner E, Todt W (2000) Zircon ages and Nd isotopic and chemical compositions of orthogneisses from the Black Forest, Germany: evidence for a Cambrian magmatic arc. Int J Earth Sci 88:791–802

Cocherie A, Baudin T, Autran A, Guerrot C, Fanning MC, Laumonier B (2005) U–Pb zircon (ID-TIMS and SHRIMP) evidence for the early Ordovician intrusion of metagranites in the late Proterozoic Canaveilles Group of the Pyrenees and the Montagne Noire (France): new U–Pb zircon datings. Bull Soc géol Fr 176:269–282

Colonna V, Piccarreta G (1975) Metamorfismo di alta pressione/bassa temperatura nei micascisti di Zangarona-Ievoli-Monte Dondolo (Sila Piccola, Calabria). Boll Soc Geol Ital 94:17–25

Compston W, Williams IS, Meyer CE (1984) U–Pb geochronology of zircons from lunar breccia 73217 using a sensitive high mass resolution ion microprobe. Proceedings of the 14th Lunar and Planetary Scientific Conference, Part 2. Geophys Res 89B:525–534

Del Moro A, Fornelli A, Piccarreta G (2000) Tectonothermal history of the Hercynian continental crust of the Serre (southern Calabria, Italy) monitored by Rb/Sr biotite resetting. Terra Nova 12:239–244

Deloule E, Alexandrov P, Cheilletz A, Laumonier B, Barbey P (2002) In situ U/Pb zircon ages for Early Ordovician magmatism in the eastern Pyrenees, France: the Canigou orthogneisses. Int J Earth Sci 91:398–405

De Paolo DJ, Wasserburg GJ (1976) Nd isotopic variations and petrogenetic models. Geophys Res Lettera 3:249–252

Dietrich D (1988) Sense of overthrust shear in the Alpine nappes of Calabria (southern Italy). J Struct Geol 10:373–382

Dörr W, Fiala J, Vejnar Z, Zulauf G (1998) U–Pb zircon ages and structural development of metagranitoids of the Tepla crystalline complex: evidence for pervasive Cambrian plutonism within the Bohemian massif (Czech Republic). Geol Rundsch 87:137–149

Dörr W, Finger F, Linnemann U, Zulauf G (2004) The Avalonian–Cadomian Belt and related peri-Gondwanan Terranes. Spec Iss Int J Earth Sci 93:657–944

Eichhorn R, Höll R, Loth G, Kennedy A (1999) Implications of U–Pb SHRIMP zircon data on the age and evolution of the Felbertal tungsten deposit (Tauern window, Austria). Int J Earth Sci 88:496–512

Fernandez-Suarez J, Gutierrez-Alonso G, Jenner GA, Tubrett MN (2000) New ideas on the Proterozoic-Early Paleozoic evolution of NW Iberia: insights from U–Pb detrital zircon ages. Precambrian Res 102:185–206

Festa V, Di Battista P, Caggianelli A, Liotta D (2003) Exhumation and tilting of the late-Hercynian continental crust in the Serre Massif (Southern Calabria, Italy). Boll Soc Geol It 2:79–88

Festa V, Messina A, Paglionico A, Piccarreta G, Rottura A (2004) Pre-Triassic history recorded in the Calabria–Peloritani segment of the Alpine chain, southern Italy. An overview. Spec Iss 2: a showcase of the Italian research in metamorphic petrology. Period Mineral 73:57–71

Fornelli A, Piccarreta G, Del Moro A, Acquafredda P (2002) Multistage melting in the lower crust of the Serre (Southern Italy). J Petrol 43:2191–2217

Gasquet D, Chévremont P, Baudin T, Chalot-Prat F, Guerrot C, Cocherie A, Roger J, Hassenforder B, Cheilletz A (2004) Polycyclic magmatism in the Tagragra and Kerdous-Tafeltast inliers (Western Anti-Atlas, Morocco). J Afr Earth Sci 39: 267–275

Gasquet D, Levresse G, Cheilletz A, Azizi-Samir MR, Mouttaqi A (2005) Contribution to a geodynamic resconstruction of the Anti-Atlas (Morocco) during Pan-African times with the emphasis on inversion tectonics and metallogenic activity at the Precambrian–Cambrian transition. Precambrian Res 140:157–182

Gebauer D, Williams IS, Compston W, Grunenfelder M (1989) The development of the Central European continental crust since the Early Archean based on convenctional and ion-microprobe dating of up 3,84 b.y. old detrital zircons. Tectonophys 157:81–96

Giacomini F, Bomparola RM, Grezzo C, Guldbransen H (2006) The geodynamic evolution of the Southern European Variscides: constraints from the U/Pb geochronology and geochemistry of the lower Paleozoic magmatic-sedimentary sequences of Sardinia (Italy). Contrib Mineral Petrol 152:19–42

Glodny J, Grauert B, Fiala J, Vejnar Z, Krohe A (1998) Metapegmatites in the western Bohemian massif: ages of crystallization and metamorphic overprint, as constrained by U–Pb zircon, monazite, garnet, columbite and Rb–Sr muscovite data. Geol Rundsch 87:124–134

Grandjacquet C, Mascle G (1978) The structure of the Ionian sea, Sicily and Calabria-Lucania. In: Nairn AEM, Kanes WH, Stehli FG (eds) The ocean basins and margins, 4b, pp 257–329

Guerrera F, Martin-Algarra A, Perrone V (1993) Late Oligocene–Miocene syn-late orogenic successions in Western and

Central Mediterranean Chains from the Betic Cordillera to the Southern Apennines. Terra Nova 5:525–544

Guillot F, Schaltegger U, Bertrand JM, Deloule E, Baudin T (2002) Zircon U–Pb geochronology of Ordovician magmatism in the polycyclic Ruitor Massif (Internal W Alps). Int J Earth Sci 91:964–978

Hanchar JM, Miller CF (1993) Zircon zonation patterns as revealed by cathodoluminescence and backscattered electron images: implications for interpretation of complex crustal histories. Chem Geol 110:1–13

Haskin LA, Haskin MA, Frey FA, Wildeman TR (1968) Relative and absolute terrestrial abundances of rare earths. In Ahrens LH (ed) Origin and distribution of the elements. Inter Ser Monogr Earth Sci 30:889–912

Hoskin PWO, Schaltegger U (2003) The composition of zircon and igneous and metamorphic petrogenesis. Reviews in Mineralogy and Geochemistry 53, Mineralogical Society of America, Washington, pp 27—62

Innocent C, Michard A, Guerrot C, Hamelin B (2003) Datation U–Pb sur zircons à 548 Ma de leptynites des Maures centrales. Signification géodynamique des complexes leptyno-amphibolitiques de l'Europe varisque. Bull Soc géol Fr 174:585–594

Jegouzo P, Peucat JJ, Audren C (1986) Caractérisation et signification géodynamique des orthogneiss calco-alcalins d'âge ordovicien de Bretagne méridionale. Bull Soc géol Fr 5:839–848

Kröner A, Willner AP, Hegner E, Frischbutter A, Hoffmann J, Bergner R (1995) Latest Precambrian (Cadomian) zircon ages, Nd isotopic systematics and P-T evolution of granitoid orthogneisses of the Erzgebirge, Saxony and Czech Republic. Geol Rundsch 84:437–456

Lahondére D, Thiéblemont D, Goujou JC, Le Métour J, Barbey P, Bronner G, Deschamps M, Cocherie A, Guerrot C, Marchand J (2004) Evolution archéenne à paléoprotérozoïque de la Dorsale de Rgueïbat (Nord de la Mauritanie). 20th Coll Afr Geol, Orléans, Abstract, p 251

Laumonier B, Autran A, Barbey P, Cheilletz A, Baudin T, Cocherie A, Guerrot C (2004) Conséquences de l'absence de socle cadomien sur l'âge et la signification des séries pré-varisques (anté-ordovicien supérieur) du sud de la France (Pyrénées, Montagne Noire). Bull Soc géol Fr 175:643–655

Liégeois JP, Berza T, Tatu M, Duchesne JC (1996) The Neoproterozoic Pan-African basement from the Alpine Lower Danubian nappe system (South Carpathians, Romania). Precambrian Res 80:281–301

Ludwig KR (2003) User's manual for a geochronological toolkit for microsoft excel. Berkeley Geochronology Center, Spec Publ No. 4

Mallard LD, Rogers JJW (1997) Relationship of Avalonian and Cadomian terranes to Grenville and Pan-African events. J Geodynamics 23:197–221

McDonough WF, Sun S (1995) The composition of the Earth. Chem Geol 120:223–253

Muller B, Klotzli US, Flisch M (1995) U–Pb and Pb–Pb zircon dating of the older orthogneiss suite in the Silvretta nappe, eastern Alps: Cadomian magmatism in the upper Austro-Alpine realm. Geol Rundsch 84:457–465

Muller B, Klotzli U, Schaltegger U, Flisch M (1996) Early Cambrain oceanic plagiogranite in the Silvretta Nappe, eastern Alps: geochemical, zircon U–Pb and Rb–Sr data from garnet-horneblende-plagioclase gneisses. Geol Rundsch 85:822–831

Murphy JB, Gutierrez-Alonso G, Nance RD, Fernandez-Suarez J, Keppie JD, Quesada C, Strachan RA, Dostal J (2006) Origin of the Rheic Ocean: rifting along a neoproterozoic suture? Geol Soc Am 34(5):325–328

Neubauer F, Frisch W, Hansen BT (2002) Early Paleozoic tectonothermal events in basement complex of the eastern Greywacke Zone (Eastern Alps: evidence from U–Pb zircon data. Int J Earth Sci 91:775–786

Ochsner A (1993) U–Pb geochronology of the Upper Proterozoic–Lower Paleozoic geodynamic evolution in the Ossa-Morena Zone (SW Iberia): constraints on the timing of the Cadomian Orogeny. Unpublished Ph.D. Thesis, ETH, Zürich

Paglionico A, Piccarreta G (1976) Le Unità del Fiume Pomo e di Castagna nelle Serre Settentrionali (Calabria). Boll Soc Geol It 95:27–37

Pearce JA (1983) Role of the sub-continental lithosphere in magma genesis at active continental margins. In: Hawkesworth CJ, Norry MJ (eds) Continental basalts and mantle xenoliths. Shiva Geology Series, Nantwich, pp 230–249

Peucat JJ, Mahdjoub Y, Drareni A (1996) U–Pb and Rb–Sr geochronological evidence for late Hercynian tectonic and Alpine overthrusting in Kabylian metamorphic basement massifs (northeastern Algeria). Tectonophys 258:195–213

Piccarreta G (1981) Deep-roted overthrusting and blue-schists metamorphism in compressive continental margin. An example from Calabria (Southern Italy). Geol Mag 118:539–544

Pin C, Lancelot JR (1978) Un exemple de magmatisme cambrien dans le Massif Central : les métadiorites quartziques intrusives dans la série du Lot. Bull Soc géol Fr XX-2:203–208

Platt JP, Compagnoni R (1990) Alpine ductile deformation and metamorphism in a Calabrian basement nappe (Aspromonte, south Italy). Ecol Geol Helv 83:41–58

Prosser G, Caggianelli A, Rottura A, Di Battista P, Del Moro A (2003) Strain concentration in the marble layers along the Palmi shear zone (Calabria, southern Italy). Geoacta 2:155–166

von Raumer JF, Stampfli GM, Borel GD, Bussy F (2002) Organization of pre-Variscan basement areas at the north-Gondwanan margin. Int J Earth Sci 91:35–52

von Raumer JF, Stampfli GM, Bussy F (2003) Gondwana-derived microcontinents—the constituents of the Variscan and Alpine collisional orogens. Tectonophys 365:7–22

Roger F, Respaut JP, Brunel M, Matte P, Paquette JL (2004) Premiére datation U–Pb des orthogneiss oeillés de la zone axiale de la Montagne Noire (Sud du Massif central): nouveaux témoins du magmatisme ordovicien dans la chaîne varisque. C R Geosci 336:19–28

Samson SD, D'Lemos RS, Miller BV, Hamilton MA (2005) Neoproterozoic paleogeography of the Cadomia and Avalon terranes: constraints from detrital zircon U–Pb ages. J Geol Soc Lond 162:65–71

Santos Zalduegui JF, Schärer U, Gil Ibarguchi JI (1995) Isotope constraints on the age and origin of magmatism and metamorphism in the Malpica-Tuy allochthon, Galicia, N-W Spain. Chem Geol 121:91–103

Schaltegger U, Gebauer D (1999) Pre-Alpine geochronology of the Central, Western and Southern Alps. Schweiz Mineral Petrogr Mitt 79:79–87

Schenk V (1980) U–Pb and Rb–Sr radiometric dates and their correlation with metamorphic events in the granulite-facies basement of the Serre, Southern Calabria (Italy). Contrib Mineral Petrol 73:23–38

Schenk V (1990) The exposed crustal cross section of southern Calabria, Italy: structure and evolution of a segment of Hercynian crust. In: Salisbury MH, Fountain DM (eds) Exposed cross-sections of the continental crust. Kluwer, Netherlands, pp 21–42

Schenk V, Todt W (1989) Age of formation of the southern Calabrian crust. Terra Abstracts 1:350

Senesi G (1999) Petrologia della zona di bordo delle plutoniti delle Serre (Catanzaro, Calabria). Unpublished Ph.D. Thesis, University of Bari, pp 1–80

Stacey JS, Kramers JD (1975) Approximation of terrestrial lead isotope evolution by a two-stage model. Earth Planet Sci Lett 26:207–221

Stampfli GM, Borel GD (2002) A plate tectonic model for the Paleozoic and Mesozoic constrained by dynamic plate boundaries and restored synthetic oceanic isochrons. Earth Planet Sci Lett 196:17–33

Sun SS (1980) lead isotopic study of young volcanic rocks from mid-ocean ridges; ocean islands and island arcs. Phil Trans R Soc Lond A 297:409–445

Thomas RJ, Chevallier LP, Gresse PG, Harmer RE, Eglington BM, Armstrong RA, de Beer CH, Martini JEJ, de Kock GS, Macey PH, Ingram BA (2002) Precambrian evolution of the Sirwa Window, Anti-Atlas Orogen, Morocco. Precambrian Res 118:1–57

Thomson SN (1994) Fission track analysis of the crystalline basement rocks of the Calabrian Arc, soutehrn Italy: evidence of Oligo-Miocene late-orogenic extension and erosion. Tectonophys 238:331–352

Tichomirowa M, Berger HJ, Koch EA, Belyatsky BV, Gotze J, Kempe U, Nasdala L, Schaltegger U (2001) Zircon ages of high-grade gneisses in the Eastern Erzgebirge (Central European Variscides)—constraints on origin of the rocks and Precambrian to Ordovician magmatic events in the Variscan foldbelt. Lithos 56:303–332

Trombetta A, Cirrincione R, Corfu F, Mazzoleni P, Pezzino A (2004) Mid-Ordovician U–Pb ages of porphyroids in the Peloritan Mountains (NE Sicily): paleogeographical implications for the evolution of the Alboran microplate. J Geol Soc Lond 161:265–276

Turniak K, Mazur S, Wysoczanski R (2000) SHRIMP zircon geochronology and geochemistry of the Orlica–Snieznik gneisses (Variscan belt of Central Europe) and their tectonic implications. Geodinamica Acta 13:293–312

Valverde-Vaquero P, Dunning GR (2000) New U–Pb ages for Early Ordovician magmatism in Central Spain. J Geol Soc Lond 157:15–26

Vavra G, Gebauer D, Schmid R, Compton W (1996) Multiple zircon growth and recrystallization during polyphase Late Carboniferous to Triassic metamorphism in granulite of Ivrea Zone (Southern Alps): an ion microprobe (SHRIMP) study. Contrib Mineral Petrol 122:337–358

Vavra G, Schmid R, Gebauer D (1999) Internal morphology, habit and U–Th–Pb microanalysis of amphibolite-to-granulite facies zircons: geochronology of the Ivrea Zone (Southern Alps). Contrib Mineral Petrol 134:380–404

Walsh GJ, Aleinikoff J, Benziane F, Yazidi A, Armstrong TR (2002) U–Pb zircon geochronology of the palaeoproterozoic tagragra de tata inlier and its neoproterozoic cover, western Anti-Atlas, Morocco. Precambrian Res 117:1–20

Wiedenbeck M, Allé P, Corfu F, Griffin WL, Meier M, Oberli F, Von Quadt A, Roddick JC, Spiegel W (1995) Three natural zircon standards for U–Th–Pb, Lu–Hf, trace elements and REE analyses. Geostand Newl 19:1–23